J. Fluid Mech. (1997), *vol.* 352, *pp.* 135–159. Printed in the United Kingdom

The PVC technique – a method to estimate the dissipation length scale in turbulent flows

By CHIH-MING HO[1] AND YITSHAK ZOHAR[2]

[1] Department of Mechanical, Aerospace & Nuclear Engineering, University of California at Los Angeles, Los Angeles, CA 90024-1597, USA

[2] Department of Mechanical Engineering, Hong Kong University of Science & Technology, Clear Water Bay, Kowloon, Hong Kong

(Received 17 February 1997 and in revised form 9 July 1997)

A time-averaged length scale can be defined by a pair of successive turbulent-velocity derivatives, i.e. $[\mathrm{d}^n u(x)/\mathrm{d}x^n]'/[\mathrm{d}^{n+1}u(x)/\mathrm{d}x^{n+1}]'$. The length scale associated with the zeroth- and the first-order derivatives, u'/u'_x, is the Taylor microscale. In isotropic turbulence, this scale is the average length between zero crossings of the velocity signal. The average length between zero crossings of the first velocity derivative, i.e. u'_x/u'_{xx}, can be reliably obtained by using the peak-valley-counting (PVC) technique. We have found that the most probable scale, rather than the average, equals the wavelength at the peak of the dissipation spectrum in a plane mixing layer (Zohar & Ho 1996). In this study, we experimentally investigate the generality of applying the PVC technique to estimate the dissipation scale in three basic turbulent shear flows: a flat-plate boundary layer, a wake behind a two-dimensional cylinder and a plane mixing layer. We also analytically explore the quantitative relationships among this length scale and the Kolmogorov and Taylor microscales.

1. Introduction

Turbulent shear flows are known to contain eddies of various scales ranging from organized large-scale to random small-scale structures. It has been shown (Tennekes & Lumley 1972) that the Navier–Stokes equations derived for steady homogeneous pure shear flow can be reduced by using the Reynold decomposition to

$$-\overline{u_i u_j} S_{ij} = 2\nu \overline{s_{ij} s_{ij}}. \tag{1.1}$$

This equation states that the rate of turbulent energy production by Reynolds stresses equals the rate of viscous dissipation. Furthermore, scaling arguments suggest that the production, i.e. extraction of kinetic energy from the mean flow, enters the turbulence mainly at large scales, but the viscous dissipation of turbulent energy occurs mainly at small scales. The existence of the energy-containing eddies within the shear region was recognized by Crow & Champagne (1971) as well as Brown & Roshko (1974). The development of a mixing layer is dominated by two sets of large organized structures: the primary, spanwise vortices and the streamwise, counter-rotating vortex pairs (Roshko 1981). These coherent structures control the mass and momentum transfer across the shear region and consequently the growth of the layer (Winant & Browand 1974). For more than a decade, the spanwise vortical structures have been studied in detail by many investigators in various turbulent shear flows: mixing layers (Ho & Huang 1982), wakes (Wygnanski, Champagne & Marasli 1986) and boundary layers

(Brown & Thomas 1977). In addition to the spanwise vortical structures, Konrad (1976) reported the existence of streamwise streaks in a mixing layer. In general, the spanwise structures are formed as a result of essentially a two-dimensional instability mechanism (Monkewitz & Huerre 1982), while the streamwise structures seem to result from three-dimensional instability of the spanwise vortical structures (Pierrehumbert & Widnall 1982). Since instability mechanisms are highly sensitive to initial conditions, the evolution of these structures can be manipulated by external excitation (Ho & Huang 1982). For surveys of the research on large-scale structures one may consult the reviews by Cantwell (1981) for bounded and by Ho & Huerre (1984) for free shear layers. It is well established now that the irrotational fluid is engulfed into the shear layer by the evolving organized structures, thus extracting energy from the mean flow, but the mixing process of the engulfed fluid takes place on smaller scales. Indeed, the energy of the large eddies cannot grow indefinitely and (1.1) has indicated that it stays bounded due to the viscous dissipation of kinetic energy by very fine eddies.

Initially laminar shear layers eventually become turbulent in a process known as the small-scale transition. The energy cascade model argues that the energy is progressively transferred from the large scales where it is injected to the smaller size eddies (Lesieur 1987). Analysis of the vorticity equation under the same conditions of (1.1) leads to the approximation (Tennekes & Lumley 1972)

$$\overline{\omega_i \omega_j s_{ij}} = \nu \overline{\frac{\partial \omega_i}{\partial x_j} \frac{\partial \omega_i}{\partial x_j}}. \tag{1.2}$$

This implies that the energy is transferred to the small scales by vortex straining, stretching or compression, and the dissipation rate of kinetic energy is proportional to the mean-square of the vorticity fluctuations. Liu (1981) showed that when the large-scale disturbance reaches its maximum, there is a significant energy transfer from the mean flow to the fine-scale motion. However, the exact mechanism by which the small scales are generated is not known yet. Until the mid 1960s, the fine-scale activity was extensively studied, theoretically and experimentally, utilizing traditional statistical methods only (Hinze 1975). This was the result of the complicated nature of and the difficulties encountered in detecting fine eddies. Nevertheless, the important role of these dissipative eddies in the mixing process was demonstrated by Briedenthal (1981), who reported that the small-scale transition is highly correlated with a sharp increase in the mixedness of the shear layer. Major progress in data-acquisition techniques coupled with significant advances in understanding large-scale eddies has opened new possibilities for studying the fine-scale activity. Huang (1985) and Hsiao (1985) developed a new scheme, peak-valley counting (PVC), for the direct detection of the small-scale structures, which was further improved by Zohar (1990). Huang (1985) reported that the small-scale activity in a plane mixing layer starts during the vortex merging and appears in the new vortex core, in the tested Reynolds number range. Huang & Ho (1990) found that the small-scale transition in their mixing layer started after the first spanwise vortex merging at the streamwise vortex cores. These studies seem to suggest that the small eddies in free-shear flows are generated as a result of the strain field, which is developed due to the interaction between the spanwise and the streamwise vortices (Ho & Huerre 1984). Likewise, Acarlar & Smith (1987) observed that in a boundary layer the lift-up of the streamwise vortices by the spanwise vortical structures may lead to the bursting phenomenon, which is associated with fine-scale production. Moser & Rogers (1993) reported that the transition process in a temporal mixing layer is associated with intense vortex stretching developed during vortex merging. Indeed, in an earlier numerical study, Brachet *et al.* (1983) showed that a

single large-scale structure subject to only a straining field can break down to smaller scales, and they speculated that it may be due to the vortex straining mechanism.

Zohar & Ho (1996) studied the small-scale activity in a plane mixing layer utilizing the PVC technique. They found that the most-probable length scale of the streamwise velocity fluctuations is equal to the scale of maximum dissipation. Foss (1994) applied the PVC technique to all three velocity components in a mixing layer, and found that the most-probable length scale is the same in all directions. A similar finding was reported by Zohar *et al*. (1990) who applied a two-dimensional version of the PVC technique to the velocity field of a numerically computed, temporal mixing layer. These results suggest that the most-probable length scale of the velocity fluctuations, as determined by the PVC technique, is equal to the length scale of the dissipation process in turbulent shear flows in general. The purpose of this paper is therefore to check the validity of this hypothesis in various turbulent flows.

2. Experimental arrangements

In the present study, experiments were carried out in three types of turbulent flows: two free shear flows, namely a plane mixing layer and a plane wake, and one wall-bounded shear flow, a plane boundary layer. It was established that all the flows were fully developed under the conditions of measurements. The time-averaged velocity, U, and the fluctuating streamwise velocity, $u(t)$, were measured by a single-wire probe of 2.5 μm in diameter. The 0.5 mm long hot wire was made of Pt-Rd. The constant-temperature anemometer had a flat frequency response up to about 30 kHz. The analog output of the anemometer was digitized with a personal-computer-based data acquisition system. The 12-bit A/D converter allowed a maximum sampling rate of 1 MHz. The actual sampling time was adjusted for each flow: 40, 20 and 6 μs for the boundary layer, wake and mixing layer respectively. For calibration, the hot wire was placed in the free stream, well outside the shear layer, along with a Pitot tube. The anemometer output voltage and the output of the pressure transducer connected to the Pitot tube were recorded. A fourth-order polynomial was fit to seven calibration velocities, using the least-squares method, to determine the five coefficients.

2.1. *Boundary layer*

A closed-return wind tunnel, details of which were reported by Blackwelder & Haritonidis (1983), was used for the boundary-layer study. The test section had a cross-sectional area of 60×90 cm^2 and was 6 m long. A 90×600 cm^2 flat plate was vertically mounted in the test section. The leading edge of the flat plate was rounded and a trailing-edge flap was installed to control the stagnation point at the leading edge. The turbulence level within the test section was less than 0.05 % at all free-stream velocities, up to 18 m s^{-1}. The laminar boundary layer which developed over the flat plate was tripped with two staggered rows of 7 mm high inverted rivets spaced 2 cm apart. The centre of the two rows, with a streamwise separation of 2 cm, was located 45 cm downstream from the leading edge.

The free-stream velocity was $U_\infty = 500$ cm s^{-1}, which is one of the cases reported by Blackwelder & Haritonidis (1983). The measurements were taken at $x = 500$ cm from the trailing edge, where a standard boundary layer was obtained as shown in figure 1(*a*). The transverse coordinate is normalized by the viscous length scale, $\nu/u_\tau = 0.075$ mm. The friction velocity, u_τ, is based on the velocity gradient at the wall, $u_\tau = [\nu(\partial U/\partial y)_{wall}]^{1/2} = 20$ cm s^{-1}, and ν is the kinematic viscosity. From the mean-velocity profile it is ascertained that the mean velocity at $Y^+ = yu_\tau/\nu = 15$ was $12u_\tau$.

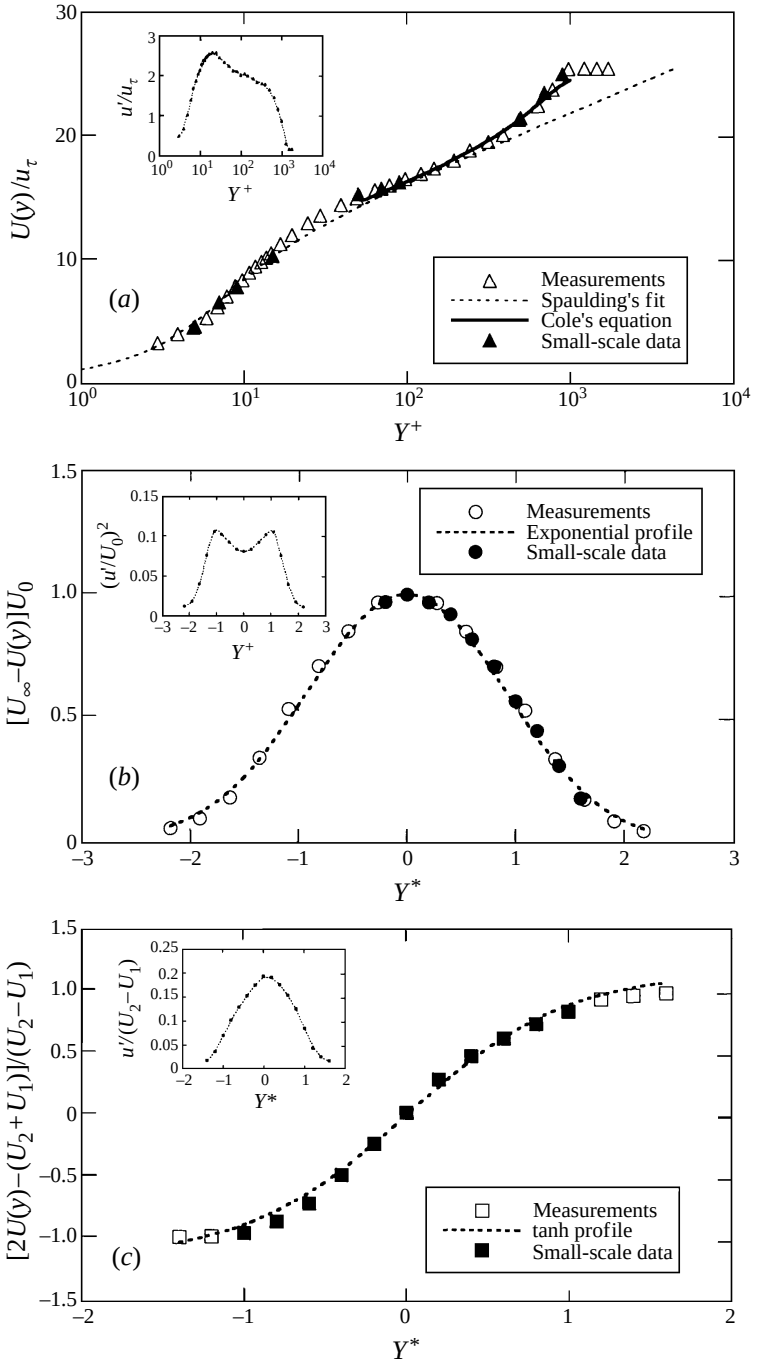

FIGURE 1. Shear layer mean and fluctuations velocity profiles: (*a*) boundary layer; (*b*) wake; (*c*) mixing layer.

This criterion was used to determine the origin, $y = 0$. Once the fully developed state of the boundary layer was established, the small-scale activity was then examined at the 10 positions marked in figure 1(*a*).

2.2. *Wake*

The wake was generated in a closed-return wind tunnel which is described by Motohashi & Blackwelder (1983). A 1.3 cm thick aluminium plate, 550 cm long and 133 cm wide was mounted horizontally on the upper side of the octagonal cross-section. The wake generator used in this study was a circular cylinder made of steel. The cylinder, 8 mm in diameter, spanned the test section and was mounted under adequate tension to ensure that it was straight and rigid.

The free-stream velocity was $U_\infty = 1300$ cm s^{-1} with turbulence level of about 0.1 %. Wygnanski *et al.* (1986) reported that the wake obeys the similarity scaling for $x > 400d$, where $d = 2\theta$ is the cylinder diameter and θ is the momentum thickness. Therefore, the small-scale activity in the wake was examined at $x = 400d$ for which the mean and r.m.s. velocity profiles are shown in figure 1(*b*). The 10 positions where the small-scale activity was examined are also marked. The transverse coordinate is normalized by the distance from the centre to where the mean velocity is equal to half of the wake deficit, $b(x)$, such that $Y^* = y/b(x)$.

2.3. *Mixing layer*

The mixing layer was studied in an open loop wind tunnel; its turbulence properties were documented by Browand & Latigo (1979). A 3×3 m^2 stilling chamber was divided into two independent sections by a 10 cm thick splitter plate. At the end of the contraction section, a steel plate was attached to the end of the splitter plate to divide the test section into two streams, each 30.5 cm deep and 91.4 cm wide. In order to obtain different velocities in the two streams, a cloth mesh was placed over the upper entrance to the stilling chamber to produce the required pressure drop for a desired velocity ratio. The experiments were conducted with laminar boundary layers on both sides of the splitter plate; the turbulence level in the vicinity of the trailing edge was about 0.3 %. The free-stream velocities were $U_1 = 2.75$ m s^{-1} and $U_2 = 12.65$ m s^{-1}, with spanwise uniformity to within 0.35 % of the maximum velocity in either stream. The velocity ratio is therefore $R = (U_2 - U_1)/(U_2 + U_1) = 0.64$. The streamwise coordinate is normalized by the initial instability wavelength, $\Lambda_0 = 3$ mm, and the velocity ratio, R, such that $X^* = Rx/\Lambda_0$. The cross-stream coordinate is normalized by the local velocity thickness, $Y^* = y/\delta(x)$, where $\delta(x) = (U_2 - U_1)/(\partial U/\partial y)_{max}$. Zohar & Ho (1996) reported that for $X^* > 6$ the velocity profiles at these conditions become self-similar. Therefore, measurements were made further downstream at $X^* = 8$, where the shear layer was fully developed. The mean and r.m.s. velocity profiles are shown in figure 1(*c*), where the locations selected for the small-scale study are marked as well.

3. A summary of the peak-valley-counting (PVC) technique

Velocity traces consist of low-frequency high-amplitude fluctuations pertaining to the passage of the coherent structures and high-frequency low-amplitude fluctuations which are assumed to be the signature of the fine eddies. Clearly, one can gain more information about the smaller scales by correctly resolving these high-frequency fluctuations. Consequently, a new peak-valley-counting technique was developed to identify every local maximum and every local minimum associated with the high-

frequency fluctuations. The PVC algorithm is designed to generate a reliable pulse train corresponding to the local extrema in the velocity signal recorded by a hot wire, thus providing an efficient method for detecting fine structures within the limits of the hot-wire anemometry.

3.1. *Small-scale resolution*

The hot-wire anemometer has a finite spatial resolution and a finite time response. Therefore, two parameters had to be adjusted to ensure the registration of most of the small scales by the hot wire. The frequency response of the anemometer is flat up to about 30 kHz. The highest most-probable frequency of the small-scale activity, in the present study, was found in the mixing layer. Thus, by fixing the mean speed at 7.7 m s^{-1}, the most probable frequency, 12 kHz, was about 2.5 times smaller than the high end of the flat frequency response. The mixing layer at these conditions also contained the smallest most-probable length scale of the fine-scale activity, 0.65 mm. Hence, the length of the wire used for the detection of small scales was about 0.5 mm. The sampling time was selected such that at least five data points were recorded per one fine eddy of the most-probable scale found in each flow. Thus, it was possible to distinguish between fine eddies with slightly different sizes, enabling the construction of a histogram for the small-scale activity in the shear flows. As a result, the measuring system was indeed able to resolve the majority of the fine-scale eddies examined in this study, and in particular the most-probable ones.

3.2. *Noise contamination*

The PVC scheme is very sensitive to noise contamination, which is inherent in every signal-processing technique manifested at the high frequency end of the spectrum. A procedure of five steps was developed to deal with this problem. Although the procedure is not unique, it does follow some physical reasoning as discussed next.

In the first step of the algorithm, a pulse of $(+1)$ is assigned to every local maximum and (-1) to every local minimum. Digitizing an analog signal introduces a finite-amplitude resolution by the A/D converter. Consequently, many peaks and valleys contain more than one data point of identical local extremum value. Therefore, it is not sufficient to decide upon a peak or valley simply by comparing it with its two adjacent data points. The separation between the examined point and the reference points increases iteratively until it is possible to sort out the character of that point. This step is successful in identifying almost all the extrema. However, it also introduces a large number of false peaks and valleys, as clearly seen in the pulse train in figure 2(*a*). Since one and only one peak can exist between a successive pair of valleys, and vice versa, the second step is designed to enforce that. Thus, in the case of two or more successive pulses with similar sign, those with smaller absolute value of the raw signal are set to zero. If the absolute value is also identical, the pulse closest to the mid-interval is kept and the rest are set to zero. This simple step eliminates more than 50% of the false pulses in most cases, as evident in figure 2(*b*).

The following steps are designed to examine a structure, a peak-valley pair, rather than a single pulse, peak or valley. In the third step, the differences between the level of each peak (or valley) and the two valleys (or peaks) next to it are calculated. The centre pulse is then set to zero, along with one of the two next to it as in the previous step, if both differences are smaller than a certain threshold. The threshold depends on the noise level introduced by the recording system: hot-wire anemometer, amplifier and A/D converter. In the present study, this threshold is found to be about 1% of the amplitude associated with an average coherent structure. After this step (see figure 2*c*) less than 20% of the pulses are false, and they seem to concentrate in regions of the

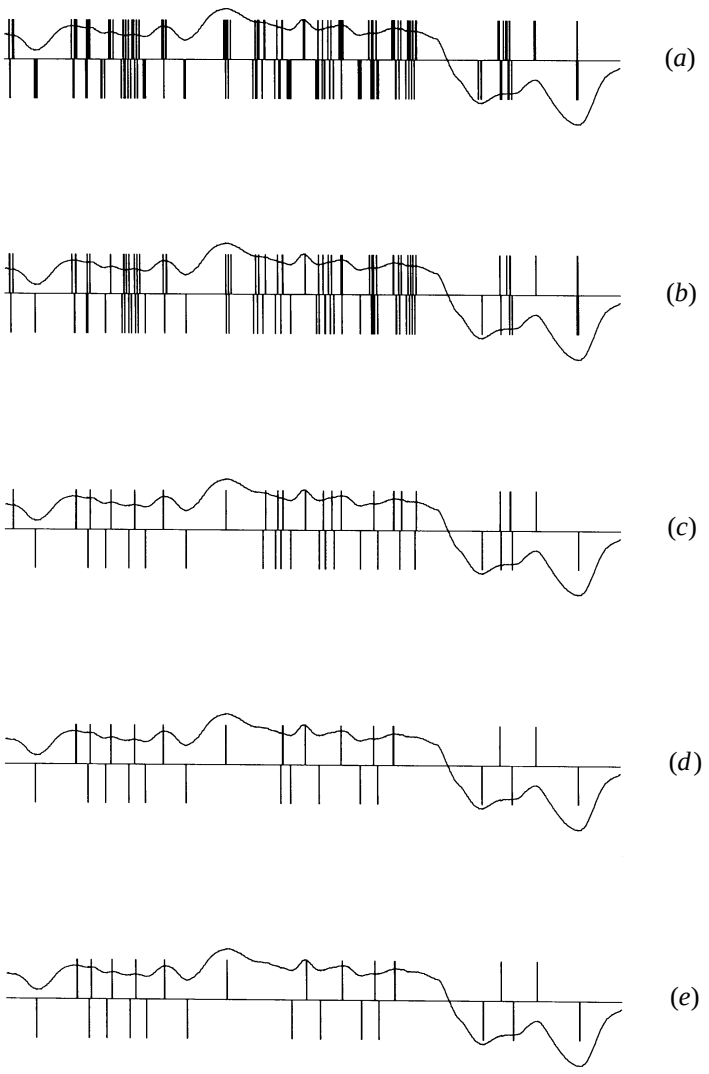

FIGURE 2. The pulse train of peaks and valleys after: (*a*) the 1st; (*b*) 2nd; (*c*) 3rd; (*d*) 4th; and (*e*) 5th stage of the PVC algorithm. (Velocity time record of 75 ms in the boundary layer at $Y^+ = 5$.)

signal where the slope is very shallow. The next step is therefore designed to improve the pulse train in those regions. Each extremum point is re-examined by comparing it with the two points which are separated by a period larger than one most-probable scale, i.e. seven data points or more. If the peak or valley is clear, i.e. greater or smaller than the two reference points, the pulse survived. Otherwise, both differences between the extremum and the two reference points are calculated, and the pulse is set to zero if both are smaller than the previous threshold. After this step (figure 2*d*) most of the remaining false pulses (about 10%) are due to the digitizing process. Hence, a combined threshold condition for frequency and amplitude is introduced to further improve the pulse train. Since at least three data points are required to resolve a structure and the digitized signal is accurate to within one bit at best, these limits are chosen for the combined threshold. Each peak-valley pair with separation time less than three sampling time units and amplitude difference less than two bits was eliminated. Finally, after applying these five steps, the number of false peaks and

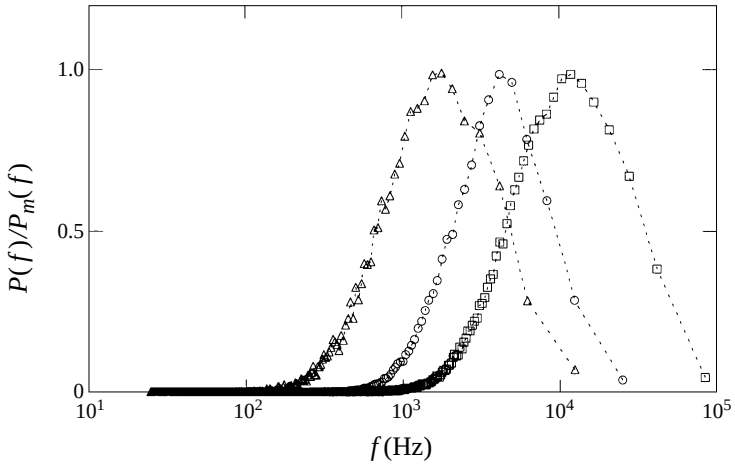

FIGURE 3. Normalized PVC histograms of: △, boundary layer at $Y^+ = 70$; ○, wake at $Y^* = 1$; □, mixing layer at $Y^* = 0$.

valleys was reduced to about 5% of the remaining pulses. Consequently, the final pulse train as shown in figure 2(*e*) seems to be a reliable tool for studying the fine-scale activity in turbulent shear flows.

3.3. *The PVC histogram and scale*

Zohar & Ho (1996) combined both the PVC and the phase-averaging techniques for registering the occurrence of every peak-valley pair in the velocity signal, in order to study the properties of the fine-scale structures such as length scales and strain rates. They reported that the most-probable length scale of the streamwise velocity fluctuations, in a plane mixing layer, is equal to the scale of maximum dissipation. It is true that while the small-scale activity is three-dimensional in nature, the velocity signal recorded by a hot wire is one-dimensional. That prompted Zohar *et al.* (1990) to apply a two-dimensional version of the PVC technique to the velocity field of a temporal mixing layer, computed numerically by Rogers & Moser (1992). They found again that the two scales corresponding to the maximum of both PVC histograms, the two- and the one-dimensional, are equal to the maximum of the dissipation spectrum. Furthermore, Foss (1994) recorded all three velocity components in a mixing layer, and reported that the corresponding microscales in all directions were about the same. Therefore, the length scale of the streamwise velocity fluctuations in all three flows will be determined using the one-dimensional PVC technique.

The PVC algorithm has been applied to the streamwise component of the velocity vector measured by a hot-wire anemometer. Thus, a pulse train of $(-1/+1)$ corresponding to the local minima/maxima in the velocity signal is constructed, as shown in figure 2(*e*). It is assumed that the time interval between each peak-valley pair (or valley-peak) represents half the period of that particular event. These time intervals are therefore doubled to yield the period of the different events, T_i, as well as their frequency, $f_i = (T_i)^{-1}$. Now, a frequency histogram can be constructed for every measurement point in each flow. It was found that the histograms reach an asymptotic shape for a population over 10^4 events. Figure 3 shows these histograms for the boundary layer, wake and mixing layer normalized by the highest probability $P_m(f)$. It is evident that in all three flows the fine-scale activity encompasses a wide range of frequencies. However, a clear peak can be seen in figure 3 for each histogram;

$f_\zeta = 2$ kHz for the boundary layer, $f_\zeta = 6$ kHz for the wake and $f_\zeta = 12$ kHz for the mixing layer.

Taylor's hypothesis is used to estimate length scales, l, in a given flow from time scales or frequencies, T or f, utilizing the appropriate convection velocity, U_c, in the transformation $l = U_c T = U_c/f$. In the mixing layer, the convection velocity of the dissipative eddies, as measured by Wygnanski & Fiedler (1970), is used. For the wake, the phase speed of the high-wavenumber range is chosen following Mattingly & Criminale (1972). In the boundary layer, the convective speed of the small scales is the local mean velocity as found by Favre, Gaviglio & Dumas (1967). The corresponding wavenumber is then calculated from the length scale, $k = 2\pi/l$. The PVC length scale, ζ, is defined as the scale for which the histogram attains its peak. Thus,

$$\zeta = \frac{U_c}{f_\zeta} \tag{3.1}$$

is the most probable scale of the fine-scale activity, which is larger than the average scale. This PVC scale is found to be 2.1 mm in the boundary layer at $Y^+ = 70$, 2.5 mm in the wake at $Y^* = 1$, and 0.65 mm in the mixing layer at $Y^* = 0$.

Essentially, the identification of local maxima/minima in the velocity signal is identical to finding the zero crossings in the signal first derivative with a negative/positive slope. Indeed, the role that the zero crossing plays in the physical description of turbulence has already been recognized (Sreenivasan, Prabhu & Narasimha 1983). However, physical measurements always contain some level of noise. Differentiating a measured signal with its noise content to obtain the zero crossings can lead to significant errors. Consequently, the latter approach yields inferior results as will be demonstrated.

4. Zero-crossing length scales in turbulent velocity signals

For a stationary random function $y = y(x)$, Rice (1945) proved the result that the zero-crossing frequency of $y(x)$, N_0, with positive (or negative) slope, is given by

$$N_0^2 = \frac{1}{4\pi^2}\frac{\overline{y_x^2}}{\overline{y^2}} \tag{4.1}$$

if $y(x)$ and $y_x(x) = \mathrm{d}y/\mathrm{d}x$ both have Gaussian distributions and are statistically independent. Similarly, Longuet-Higgins (1958) pointed out that the stationary-point frequency of $y(x)$, N_1, which is the zero-crossing frequency of $y_x(x)$, is given by

$$N_1^2 = \frac{1}{4\pi^2}\frac{\overline{y_{xx}^2}}{\overline{y_x^2}} \tag{4.2}$$

where $y_{xx}(x) = \mathrm{d}^2y/\mathrm{d}x^2$. Later, Ylvisaker (1965) proved that $2\pi N_0 = y_x'/y'$ for any continuous stationary Gaussian process $y(x)$ with finite $(2\pi N_0)^{-1}$ without invoking statistical independence between $y(x)$ and $y_x(x)$; y' and y_x' are the r.m.s. of y and y_x.

Liepmann (1949) argued that if $y(x)$ was the turbulent velocity fluctuation, $u(x)$, then N_0 could provide an indication of the viscous dissipation, which is proportional to $u_x' = u'/\lambda$. Thus, assuming normal distributions for $u(x)$ and $u_x(x)$, the Taylor microscale, λ, should be equal to $(2\pi N_0)^{-1}$. However, turbulence is inherently non-Gaussian, and Rice's results cannot automatically be expected to hold. Figures 4(*a*)–4(*c*) compare the distributions of u, u_x, and u_{xx}, respectively, in the mixing layer with normal distributions having the same standard deviations. These figures

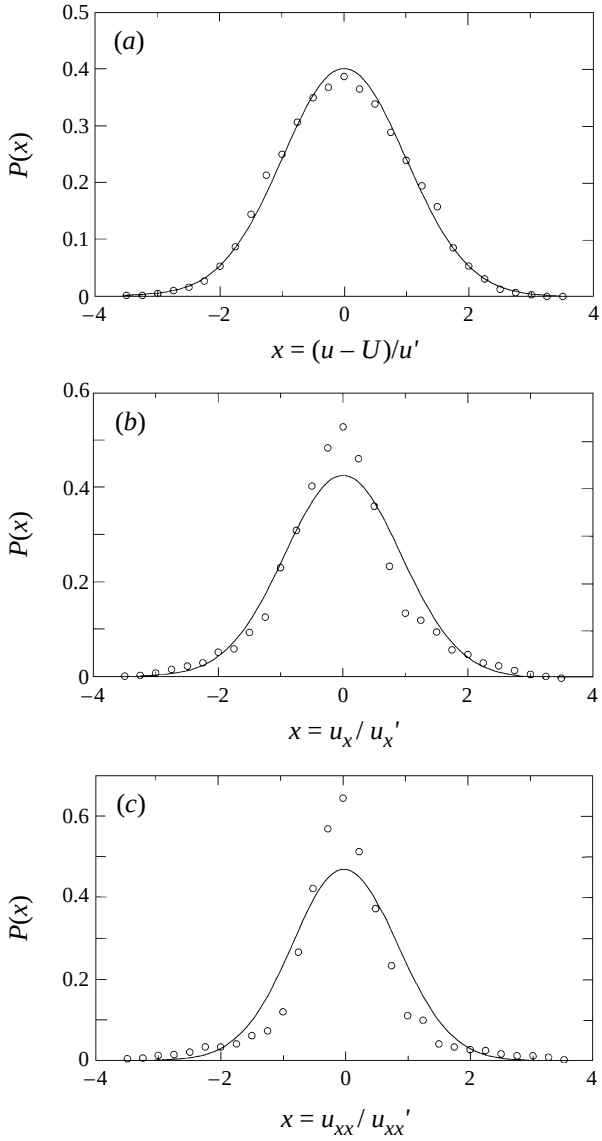

FIGURE 4. Probability distribution function in the mixing layer for: (*a*) u: ○, data; ——, Gaussian ($\sigma = 0.995$); (*b*) u_x; ○, data; ——, Gaussian ($\sigma = 0.935$); (*c*) u_{xx}: ○, data; ——, Gaussian ($\sigma = 0.855$).

qualitatively show that the distributions are not Gaussian. A measure to quantify how close a process y is to being Gaussian is its flatness factor, $\overline{y^4} = (\overline{y^2})^2$, which is exactly 3 for a normal distribution. Figure 5 shows the flatness factor in the mixing layer as a function of the derivative exponent, n, i.e. $\mathrm{d}^n u(x)/\mathrm{d}x^n$. The flatness factor increases with n from 2.7 for $P(u)$ to 5.6 for $P(u_{xx})$. Similar results were reported by Batchelor & Townsend (1949) suggesting that the higher the derivative the further the resulting signal deviates from a normal distribution.

Nevertheless, the measurements of Liepmann, Laufer & Liepmann (1951) in isotropic turbulence have shown that λ is equal to $(2\pi N_0)^{-1}$ to within 20%. The general explanation for this finding has been that the one-point p.d.f. of the velocity in

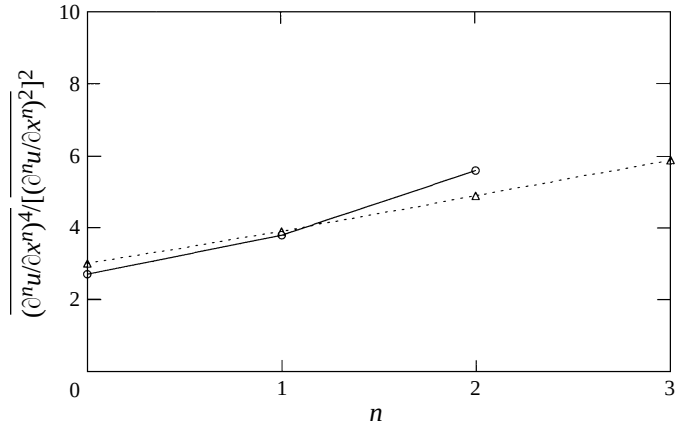

FIGURE 5. Flatness factor of streamwise-velocity derivatives in the mixing layer: —○—, present experiment; – –△– –, Batchelor & Townsend (1949).

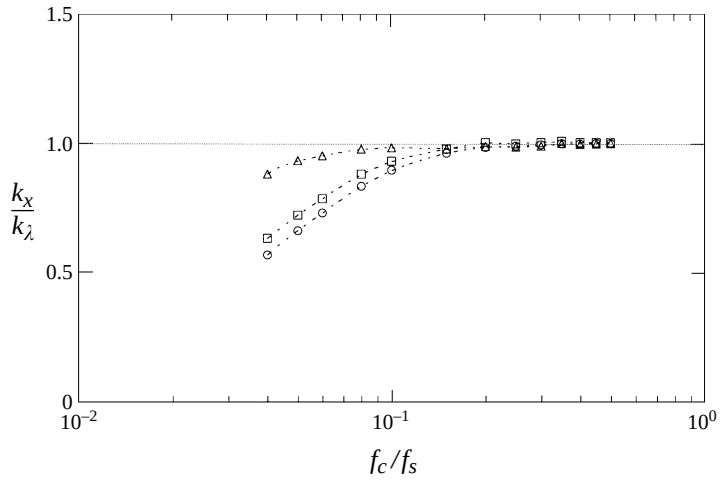

FIGURE 6. Variations of u'/u'_x with the filter cut-off frequency, f_c: △, boundary layer; ○, wake; □, mixing layer.

isotropic turbulence is not too far from being Gaussian. Indeed, figure 4(*a*) shows that $P(u)$ for which the flatness factor is 2.7 is very close to a normal distribution. However, similar findings were reported by Laufer (1950) for the streamwise velocity fluctuations in a two-dimensional channel flow, where the one-point p.d.f.'s are strongly non-Gaussian. Therefore, it seems plausible that Rice's result might have a much more general applicability than it has been proved for.

4.1. *Zero crossings of the streamwise velocity fluctuations*

Sreenivasan *et al.* (1983) carried out measurements in two boundary layers, a plane wake behind a circular cylinder and a two-dimensional channel. They showed that zero-crossing measurements can be severely affected by factors like the dynamic range of the signal, noise content and the cut-off frequency: that is, when these factors are not taken into account, misleading conclusions can be easily drawn. Sreenivasan *et al.* (1983) argued that if the signal is passed through a low-pass filter set at a frequency f_c, the zero-crossing frequency, N_0, is expected to increase initially with f_c and then attain

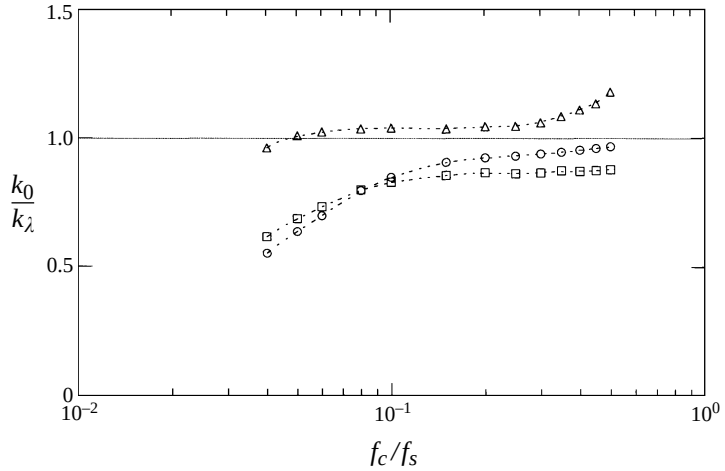

FIGURE 7. Variations of N_0 with the filter cut-off frequency, f_c: △, boundary layer; ○, wake; □, mixing layer.

a plateau, representing the true value. Further increase in the value of f_c increases the noise content; therefore at substantially higher settings of f_c, the number of zero crossings starts increasing again.

In this study, the zero-crossing approach is compared with r.m.s. calculations. The Taylor microscale, λ, is first determined by calculating the ratio u'/u'_x, or rather $U_c u'/u'_t$, after passing the signal through a low-pass filter with different cut-off frequencies. The corresponding wavenumber, $k_x = 2\pi u'_t/U_c u'$, is plotted in figure 6. In all three shear layers, k_x approaches an asymptotic value. This asymptotic value is defined here as the Taylor wavenumber, k_λ. The corresponding length scale, $\lambda = 2\pi/k_\lambda$, is the Taylor microscale: 4.95 mm for the boundary layer, 5.3 mm for the wake and 2.1 mm for the mixing layer. Figure 6 shows that in each case k_x reaches the asymptotic value of k_λ when the cut-off frequency is higher than 10 % of the sampling frequency, f_s. This indicates that the Taylor microscale, estimated directly from the recorded signal and its derivative, is not very sensitive to noise contamination.

Next, the average zero-crossing frequency of the streamwise velocity signal, N_0, is obtained. The Taylor wavenumber is now used to normalize the zero-crossing wavenumber, $k_0 = 4\pi^2 N_0/U_c$, as shown in figure 7. A clear plateau is evident for each curve as expected when the signal-to-noise ratio is reasonably good. The plateau value of $k_0/k_\lambda = (u'/u'_t)(2\pi N_0)$ is 0.9 for the mixing layer, 0.95 for the wake and 1.05 for the boundary layer. These values are consistent with the results of Sreenivasan *et al.* (1983) who obtained values of 0.9 in a plane boundary layer and 1.05 in a plane wake. So, the Taylor microscale can be estimated from the zero crossings of the turbulent velocity fluctuations according to Rice's formula although the signal is clearly non-Gaussian. However, we are interested in the dissipation length scale, and it is well known that the Taylor microscale is always larger than the dissipation length scale. Therefore, Rice's formula will now be applied to the stationary points (maxima and minima) of the signal to obtain another scale, which is expected to be smaller than the zero-crossing length scale.

4.2. *Estimation of u'_x/u'_{xx}*

Similarly to the Taylor microscale, one can define a scale based on the ratio between the r.m.s. of the first and the second velocity derivative, u'_x/u'_{xx}. However, as long as the signal is differentiable, there is an infinite number of length scales which can be

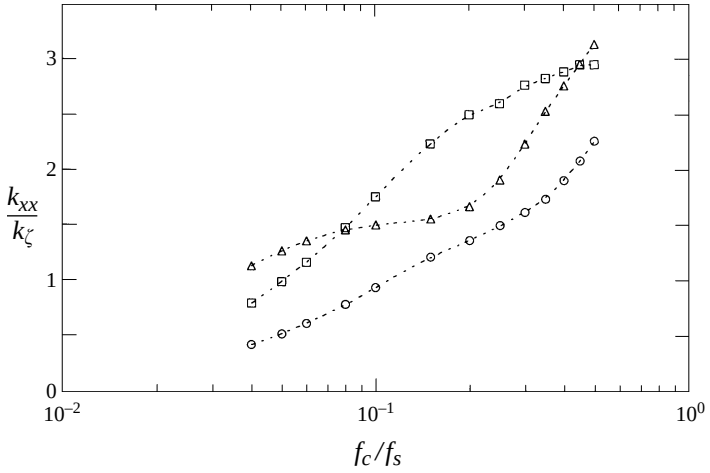

FIGURE 8. Variations of u'_x/u'_{xx} with the filter cut-off frequency, f_c: △, boundary layer; ○, wake; □, mixing layer.

defined by any pair of successive derivatives, i.e. $[\mathrm{d}^n u(x)/\mathrm{d}x^n]/[\mathrm{d}^{n+1}u(x)/\mathrm{d}x^{n+1}]$. Therefore, the introduction of another length scale has to be supported by physical arguments before attempting to calculate it. Two approaches can be considered in examining the scale u'_x/u'_{xx}: the auto-correlation and the auto-spectrum functions.

The velocity auto-correlation function in isotropic turbulence depends only on the separation distance, r:

$$\overline{u(x)\,u(x+r)} = u'^2 f(r) \tag{4.3}$$

and

$$\left(\frac{u'_x}{u'_{xx}}\right)^2 = \frac{\overline{u_x\,u_x}}{\overline{u_{xx}\,u_{xx}}} = -\frac{f_0^{\mathrm{ii}}}{f_0^{\mathrm{iv}}} \tag{4.4}$$

where f_0^{ii} and f_0^{iv} are, respectively, the second and the fourth derivative of $f(r)$ at $r = 0$. The function $f(r)$ can be expanded as follows:

$$f(r) = f_0 + \frac{f_0^{\mathrm{ii}}}{2}r^2 + \frac{f_0^{\mathrm{iv}}}{24}r^4 + \ldots \tag{4.5}$$

and so $f_0^{\mathrm{ii}} = -\lambda^{-2}$. The ratio u'_x/u'_{xx} is now given by

$$\frac{u'_x}{u'_{xx}} = \left(-\frac{f_0^{\mathrm{ii}}}{f_0^{\mathrm{iv}}}\right)^{1/2} = \left(\frac{\lambda^2}{\lambda^4 f_0^{\mathrm{iv}}}\right)^{1/2} = \frac{\lambda}{(\lambda^4 f_0^{\mathrm{iv}})^{1/2}}; \tag{4.6}$$

f_0^{iv} is unknown since there is no analytical solution for $f(r)$. However, the significance of the term $\lambda^4 f_0^{\mathrm{iv}} = \lambda^2/(u'_x/u'_{xx})^2$, can be seen in the vorticity equation derived by Batchelor & Townsend (1947):

$$\frac{\mathrm{d}\omega'^2}{\mathrm{d}t} = -\frac{7}{3\sqrt{5}}\omega'^3\lambda^3 K_0^{\mathrm{iii}} - \frac{14}{3\sqrt{5}}\omega'^3\frac{\lambda^4 f_0^{\mathrm{iv}}}{Re_\lambda}, \tag{4.7}$$

where ω' is the r.m.s. of the total vorticity and $u'^3 K_0^{\mathrm{iii}} = \overline{(\partial u/\partial x)^3}$ is the triple correlation function. This equation states that the rate of change of ω'^2 is controlled by the balance between production of vorticity due to vortex staining and dissipation of vorticity due to viscosity. Thus, the scale u'_x/u'_{xx} is found to be explicitly related to the viscous dissipation of vorticity, and so it is worth comparing it with the other scales in connection with the dissipation of kinetic energy in turbulent flows.

An attempt to solve (4.7) will inevitably lead to the closure problem, where there are more unknowns than equations. Taylor (1938) was the first to try to estimate f_0^{iv} from

his measurements of the shape of the correlation function, $f(r)$. He obtained the value of $\lambda^4 f_0^{\mathrm{iv}} = 12.5$ in grid-turbulence flow with Re_λ of about 60. Later, Batchelor & Townsend (1947) measured each of the terms in (4.7) and suggested that at large Reynolds numbers $\lambda^4 f_0^{\mathrm{iv}} = 0.2 Re_\lambda$. Hence, using the relationship between the Taylor scale and Kolmogorov scale, $\eta: \lambda/\eta = 15^{1/4} Re_\lambda^{1/2}$, (4.6) becomes

$$\frac{u_x'}{u_{xx}'} = \frac{\lambda}{(\lambda^4 f_0^{\mathrm{iv}})^{1/2}} = \frac{\lambda}{(0.2 Re_\lambda)^{1/2}} = \frac{15^{1/4}\eta}{0.2^{1/2}} = 4.401\eta. \tag{4.8}$$

This result, $u_x'/u_{xx}' = 4.4\eta$, suggests the existence of an intermediate length scale, smaller than the Taylor and larger than the Kolmogorov scale, which is relevant to the dissipation process. Therefore, it is of interest to estimate this length scale correctly, and the auto-spectrum function is examined next.

In isotropic turbulence

$$\overline{u(x)\,u(x+r)} = \int_0^\infty F_{uu}(k)\,\mathrm{e}^{\mathrm{i}kr}\,\mathrm{d}k \tag{4.9}$$

Hence,

$$\left(\frac{u_x'}{u_{xx}'}\right)^2 = \frac{\overline{u_x u_x}}{\overline{u_{xx} u_{xx}}} = \frac{\displaystyle\int_0^\infty k^2 F_{uu}(k)\,\mathrm{d}k}{\displaystyle\int_0^\infty k^4 F_{uu}(k)\,\mathrm{d}k} = \frac{\displaystyle\int_0^\infty k^2 E(k)\,\mathrm{d}k}{\displaystyle\int_0^\infty k^4 E(k)\,\mathrm{d}k} \tag{4.10}$$

and the task is to evaluate both integrals. The upper integral, $\int k^2 E(k)\,\mathrm{d}k$, is related to the dissipation rate, ϵ,

$$\epsilon = 2\nu \int k^2 E(k)\,\mathrm{d}k \tag{4.11}$$

where the dissipation rate is equal to $\epsilon = 15\nu(u_x')^2$. On the other hand, $\int k^4 E(k)\,\mathrm{d}k$ is related to $\int k^2 E(k)\,\mathrm{d}k$ as follows (Lesieur 1987):

$$\frac{\mathrm{d}}{\mathrm{d}t}\int_0^\infty k^2 E(k,t)\,\mathrm{d}k = \overline{\omega_i \omega_j \frac{\partial u_i}{\partial x_j}} - 2\nu \int_0^\infty k^4 E(k,t)\,\mathrm{d}k. \tag{4.12}$$

For the shear flows considered in this study, the production and dissipation of enstrophy are almost in equilibrium, therefore (Monin & Yaglom 1975)

$$2\nu \int_0^\infty k^4 E(k,t)\,\mathrm{d}k \approx \overline{\omega_i \omega_j \frac{\partial u_i}{\partial x_j}} = -\tfrac{35}{2}\overline{(u_x)^3} = -\tfrac{35}{2} S[\overline{(u_x)^2}]^{3/2}, \tag{4.13}$$

where S is the skewness derivative, and is of the order of -0.5 (Lesieur 1987). Hence,

$$\frac{u_x'}{u_{xx}'} = \frac{\epsilon^{1/2}}{\left(\frac{35}{4}\right)^{1/2}\left(\frac{\epsilon}{15\nu}\right)^{3/4}} = \frac{4^{1/2} 15^{3/4}}{35^{1/2}}\left(\frac{\nu^3}{\epsilon}\right)^{1/4} = 2.577\eta. \tag{4.14}$$

The auto-spectrum then yields a scale u_x'/u_{xx}' of about 2.6η. Clearly, both the auto-correlation and the auto-spectrum approaches predict that the scale u_x'/u_{xx}' is greater than the Kolmogorov scale, but the value of the ratio of the two scales is not satisfactory.

4.3. *Stationary points of the streamwise velocity fluctuations*

The stationary points of a signal are the zero crossings of its derivative. Here, the time derivative of the streamwise velocity signal, $u_t(t)$, is obtained by central differencing. The resulting signal, u_t, is passed through a low-pass filter. Again, two length scales can

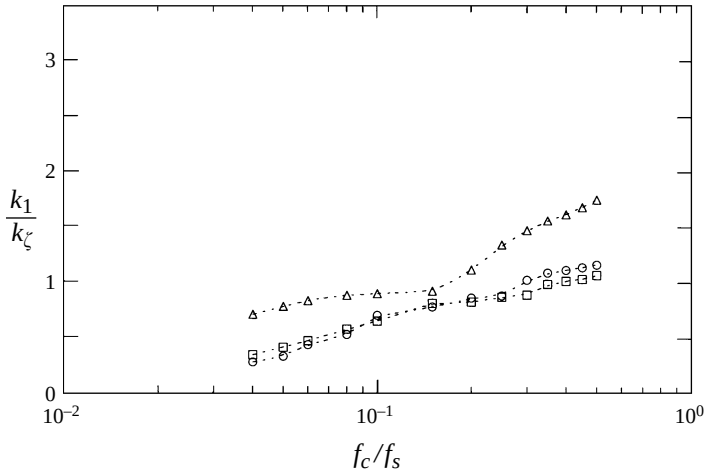

FIGURE 9. Variations of N_1 with the filter cut-off frequency, f_c: $\triangle$, boundary layer; $\bigcirc$, wake; $\square$, mixing layer.

be calculated for each cut-off frequency: one from the ratio u'_x/u'_{xx} and the other from the zero-crossing frequency, N_1. The ratio u'_x/u'_{xx} is estimated by $U_c u'_t/u'_{tt}$. The corresponding wavenumber, k_{xx}, normalized by the PVC wavenumber, $k_\zeta = 2\pi/\zeta$, is plotted in figure 8 as a function of the cut-off frequency, f_c. Unlike the asymptotic behaviour observed for k_x in all three cases (figure 6), k_{xx} is continuously increasing with f_c. This suggests that the signal-to-noise ratio is quite poor. This is expected since further differentiation of a noisy signal can only amplify the noise content. A similar pattern can be observed in figure 9, where the stationary-point wavenumber, $k_1 = 4\pi^2 N_1/U_c$, is plotted as a function of the cut-off frequency; no clear plateau can be observed in any of the three curves. Sreenivasan *et al.* (1983) have already pointed out that if the signal-to-noise ratio is low, so that the 'gap' between the high-frequency content of the signal and the noise is small, the plateau region diminishes in extent. They further argued that even if the noise is marginally higher than is acceptable in many cases, this plateau may completely disappear. So, it seems that differentiating a turbulent velocity signal, even with good signal-to-noise ratio (about 0.05 in the wake), emphasizes the noise content to such an extent that neither direct measurement of the zero-crossing frequency, N_1, nor the calculation of the ratio u'_x/u'_{xx} can yield a reliable value of the length scale. Nevertheless, figures 8 and 9 show that both k_{xx}/k_ζ and k_1/k_ζ are of order one. This indicates that it may be possible to estimate the dissipation length scale if the noise problem can be alleviated. Hence, one still would like to explore other alternatives to estimate the ratio u_t/u_{tt} in order to assess the validity of Rice's results, and this ratio in turn may provide a good estimate for the dissipation length scale. This indeed has been accomplished by developing the PVC technique and applying it to the streamwise velocity fluctuations.

5. The universality of the PVC length scale

The PVC histograms can be used to construct p.d.f.'s for the activity of the small scales using Taylor's hypothesis, $k = 2\pi f/U_c$. The p.d.f.'s, $P(k/k_\zeta)$, are obtained by normalizing the corresponding histograms such that $\int P(k/k_\zeta)\,\mathrm{d}(k/k_\zeta) = 1$, as shown in figure 10(*a–c*) for the three shear layers. The abscissa is normalized by the wavenumber of the peak frequency, k_ζ, so that the maximum of the p.d.f. appears at $k/k_\zeta = 1$.

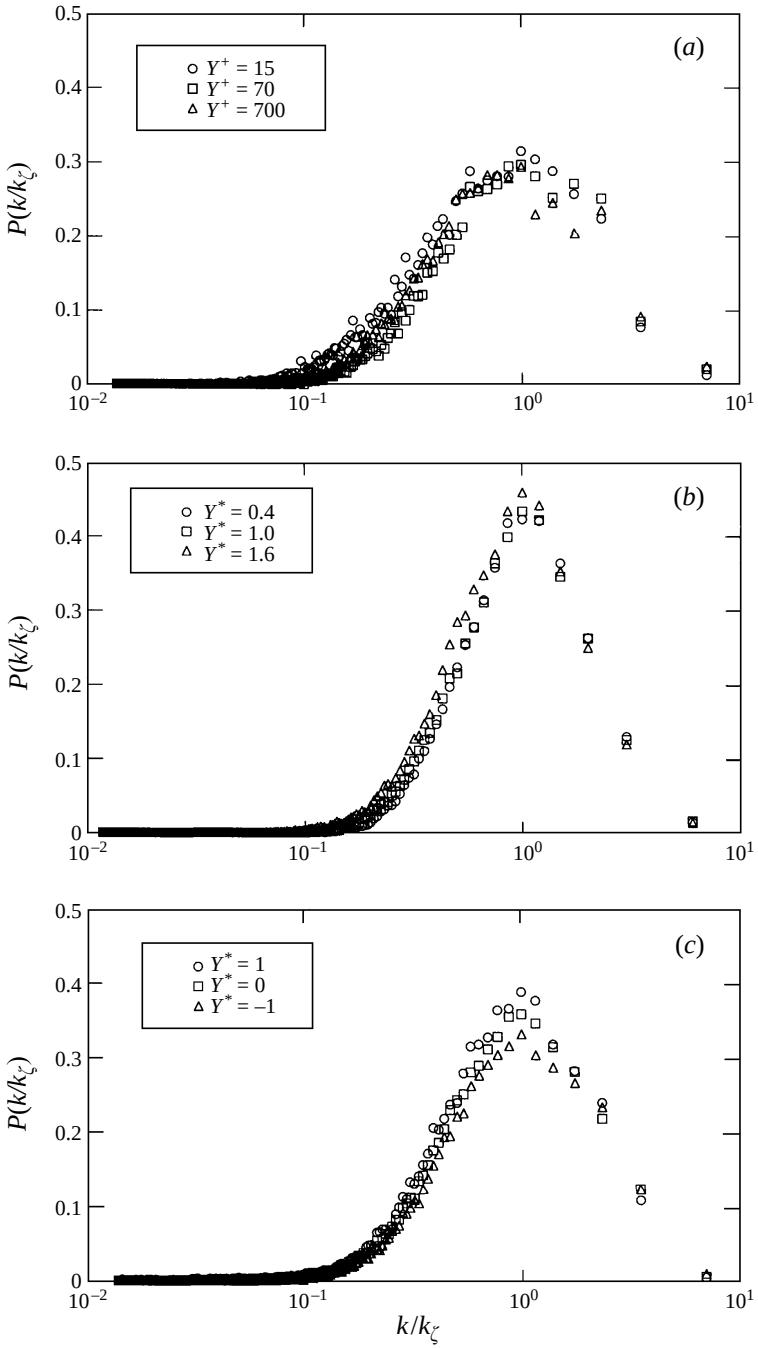

FIGURE 10. Fine-eddy p.d.f.'s for: (*a*) boundary layer; (*b*) wake; (*c*) mixing layer.

5.1. *Spatial dependence of the small-scale activity*

Huang & Ho (1990) used the PVC technique to register the instant of occurrence of the local maximum or minimum velocity in relation to the large scales in order to map out the spatial distribution of the small-scale activity inside the coherent structures. They found that the fine eddies initially appear at the core of the streamwise vortices.

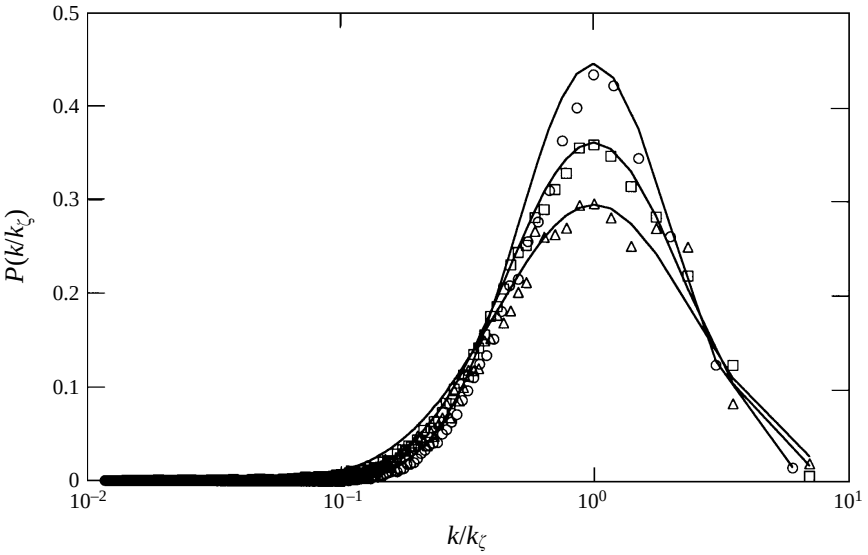

FIGURE 11. A comparison between the p.d.f.'s of the shear flows and log-normal distributions: △, boundary layer at $Y^+ = 70$ ($\sigma = 0.9$); ○, wake at $Y^* = 1$ ($\sigma = 0.7$); □, mixing layer at $Y^* = 0$ ($\sigma = 0.8$).

Similarly, Ferre *et al.* (1990) reported that intense fine-scale activity was detected in the cores of the large double-roller eddies of a plane turbulent wake. However, since all three flows under the current investigation are plane shear layers, it is expected that the statistical properties will be independent of the spanwise direction. Zohar & Ho (1996) confirmed that downstream of the small-scale transition region in a plane mixing layer the fine-scale activity becomes two-dimensional. Thus, only measurements taken at the mid-spanwise plane, $z = 0$, of the shear layers (wind tunnels) are discussed in this paper. Both, the Taylor and the Kolmogorov microscales, λ and η, are known to be weak functions of the turbulent Reynolds number, $Re_\lambda = u'\lambda/\nu$ (Batchelor 1953). Consequently, they grow very slowly with the streamwise distance. Likewise, Zohar & Ho (1996) reported that similar downstream dependence for the fine-eddy length scale, ζ, was observed in the fully developed region of a plane mixing layer. Therefore, one streamwise location was selected for each shear layer to study the small-scale activity, as described in §2.

The fine-eddy length scale is expected to vary with the cross-stream direction, since toward the edges of the shear layers the turbulence intermittency decreases as reported by Wygnanski & Fiedler (1970). Zohar & Ho (1996) reported that the most-probable length scale at both edges of the plane mixing layer was about 50% greater than the scale at the centre of the layer. However, when the fine-scale p.d.f.'s are normalized by the local most-probable wavenumber, $k_\zeta(y) = 2\pi/\zeta(y)$, they collapse onto a single curve, as shown in figure 10(*a–c*) for each of the three shear layers. This seems to suggest the existence of a self-similar state for the small-scale activity.

5.2. *Universality of the PVC length scale*

The collapse of all p.d.f.'s onto a single curve in each of the three flows when properly normalized gave hope for the existence of a universal distribution of the fine-scale eddies in all turbulent shear flows. Therefore, the p.d.f.'s of the three shear layers are compared in figure 11, where only one curve representing each layer is plotted. These are the distributions obtained at cross-stream locations deep inside the shear layers:

$Y^+ = 70$ for the boundary layer, $Y^* = 1$ for the wake and $Y^* = 0$ for the mixing layer, in order to minimize boundary effects. Moreover, since the fine-eddy wavenumber cannot have negative values and subsequently $P(k/k_\zeta) = 0$ for $(k/k_\zeta) \leqslant 0$, a log-normal distribution function is fitted for each case. The function is given by

$$P(k/k_\zeta) = \frac{1}{(2\pi)^{1/2}\sigma(k/k_\zeta)} \exp\left[-\frac{1}{2}\left(\frac{\ln(k/k_\zeta) - \mu}{\sigma}\right)^2\right], \tag{5.1}$$

where μ and σ are the mean and the standard deviation of $\ln(k/k_\zeta)$. Selecting $\mu = \sigma^2$ ensures that $\mathrm{d}P(k/k_\zeta)/\mathrm{d}(k/k_\zeta) = 0$ is at $k/k_\zeta = 1$. It is clear that although the peak distribution appears at $k/k_\zeta = 1$, due to the normalization, the value of this peak is different for each case. The exact value of the p.d.f.'s maximum is controlled by the standard deviation, σ. The best log-normal fit is obtained for $\sigma = 0.7$ in the wake, $\sigma = 0.8$ in the mixing layer and $\sigma = 0.9$ in the boundary layer. These are rather interesting results indicating a non-monotonic dependence of σ on the turbulent Reynolds number, Re_λ, since $Re_\lambda = 115$, 305 and 120 in the wake, mixing layer and boundary layer, respectively. Previous studies, e.g. Monin & Yaglom (1975), suggested that the dissipation rate has a log-normal probability distribution on similar grounds to those mentioned above. Furthermore, they assumed that the distribution variance is given by $A + \beta \ln(\Lambda/\eta)$, where Λ is the scale of the energy-containing eddies, η is the Kolmogorov microscale, and β is the universal intermittency exponent. Since $\Lambda/\eta \sim Re_\lambda^{3/2}$, one would expect the standard deviation of the dissipation-rate distribution to increase with Re_λ and similarly σ of the fine-scale eddy distribution. However, this universal behaviour becomes more apparent in flows with a very high Reynolds number, where the separation between the large- and the small-scale structures is large. Unfortunately, the turbulent Reynolds number in the flows tested here is modest, 100–300. Consequently, the small-scale activity may not be completely independent of the large-scale structures. Indeed, A is a parameter which depends on the large-scale motion. Hence, the flow macrostructure can affect the dissipation-rate distribution as well as the fine-scale distribution independent of Re_λ. It is plausible then that the different topology of the large-scale structures in the three shear layers, due to the variations in the mean shear, results in a different fine-scale activity. At the relatively low Taylor-scale Reynolds number range, we did not observe a monotonic increase of σ with Re_λ in the three shear flows. At any rate, only the mode of the p.d.f. is important to estimate the dissipation length scale and not the entire shape.

6. The relation between PVC and classical turbulence length scales

6.1. *Dissipation-spectrum estimate*

The characterization of the dissipation of kinetic energy in turbulent flows requires the estimation of the dissipation spectrum. The existence of organized structures in turbulent shear flows casts doubt on the validity of employing conventional dissipation estimates based on the assumption of local isotropy. Van Atta (1991) presented experimental data supporting Kolmogorov's hypothesis of statistical independence of large and small scales together with local isotropy of the small scales of turbulence in a homogeneous fluid. The working fluid in this study, air, is homogeneous and, hence, the conventional estimates of dissipation are employed. The dissipation spectrum, $D(k)$, can be calculated from the three-dimensional energy spectrum, $E(k)$, as follows (Batchelor 1953):

$$D(k) = k^2 E(k). \tag{6.1}$$

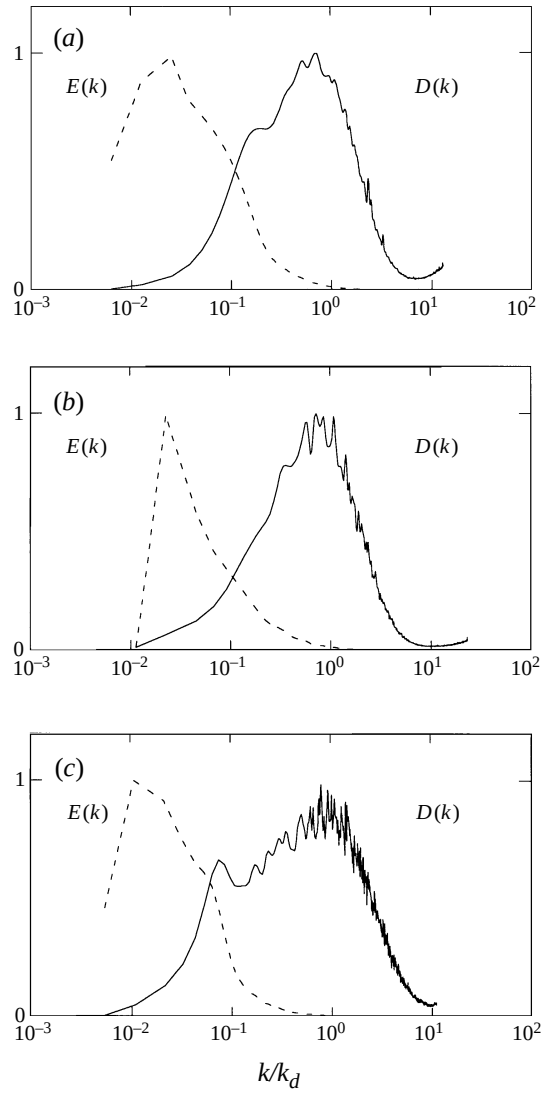

FIGURE 12. Energy, $E(k)$, and dissipation, $D(k)$, spectra for: (*a*) boundary layer at $Y^+ = 70$; (*b*) wake at $Y^* = 1$; (*c*) mixing layer at $Y^* = 0$.

Unfortunately, the three-dimensional energy spectrum cannot be measured directly. However, the one-dimensional energy spectrum, $F_{uu}(k_x)$ can be estimated from the velocity fluctuations, $u(t)$. The measuring sensor, i.e. a hot wire, has a finite spatial resolution. Therefore, the estimated energy contained within scales smaller than the sensor size has to be corrected. The procedure suggested by Wyngaard (1968) was adopted in this study to better estimate the one-dimensional energy spectrum. Assuming local isotropy, the three-dimensional energy spectrum can be calculated from the corrected one-dimensional spectrum (Batchelor 1953):

$$E(k) = k^3 \frac{\mathrm{d}}{\mathrm{d}k}\left[\frac{1}{k}\left(\frac{d}{\mathrm{d}k}F_{uu}(k)\right)\right] \tag{6.2}$$

The pair of spectra, $E(k)$ and $D(k)$, estimated for the boundary layer at $Y^+ = 70$, for the wake at $Y^* = 1$ and for the mixing layer at $Y^* = 0$, are shown in figure 12(*a–c*)

respectively; each spectrum is normalized by its maximum value. The peak of the energy spectrum, where $dE(k)/dk = 0$, corresponds to the scale of the large energy-containing eddies. Similarly, the peak of the dissipation spectrum, where $dD(k)/dk = 0$, corresponds to the scale of maximum dissipation. Thus, we define this scale as the dissipation length scale with the corresponding wavenumber, k_d, and the problem is how to evaluate it.

6.2. *Dissipation length scale*

So far, either the Kolmogorov microscale, η, or the Taylor microscale, λ, has been regarded as the dissipation length scale. An estimate of the dissipation scale can be obtained from the analysis of the structure function. In the viscous region, $r \ll \eta$, friction has a dominant effect on the relative motion. The velocity can be expanded in a Taylor series, $u(x+r) = u(x) + (\partial u/\partial x)\, r + O(r^2)$, resulting in (Monin & Yaglom 1975)

$$\overline{[u(x+r)-u(x)]^2} \approx \overline{(\partial u/\partial x)^2}\, r^2; \quad r \ll \eta. \tag{6.3}$$

On the other hand, the Kolmogorov second hypothesis in the inertial subrange, $\eta \ll r \ll \Lambda$, leads to (Monin & Yaglom 1975)

$$\overline{[u(x+r)-u(x)]^2} \approx C\epsilon^{2/3} r^{2/3}; \quad \eta \ll r \ll \Lambda, \tag{6.4}$$

where ϵ is the dissipation rate and Λ is the scale of the energy-containing eddies. If the dissipation scale is identified as the cross-over scale of the structure function, namely the distance r at which the inertial-range and Taylor-series versions of the structure function agree, then in isotropic turbulence

$$C\epsilon^{2/3} r^{2/3} = \overline{(du/dx)^2}\, r^2 = (\epsilon/15\nu)\, r^2 \tag{6.5}$$

where ν is the kinematic viscosity. With universal value $C \approx 2$ (Townsend 1976),

$$r_{cross\text{-}over} = 30^{3/4}(\nu^3/\epsilon)^{1/4} = 12.819\eta. \tag{6.6}$$

So $r_{cross\text{-}over}$ is about 13 times the Kolmogorov scale. Indeed, it is well known that the Kolmogorov microscale estimates the smallest scale of dynamical importance in fluid flows. Thus, it presents a cut-off scale for the dissipation spectrum, which is typically about one order of magnitude smaller than the scale of maximum dissipation. However, it is of interest to know the exact ratio between the two scales. If one assumes Pao's spectrum for the energy (Pao 1965), then the dissipation spectrum can be analytically expressed as

$$D(k) = 2\alpha\nu\epsilon^{2/3} k^{1/3} \exp[-\tfrac{3}{2}\alpha(k\eta)^{4/3}], \tag{6.7}$$

where α is a constant of order 1. For $\alpha = 1.5$, the peak of the dissipation spectrum occurs at $k_d/k_\eta = 0.19$, where $k_\eta = 2\pi/\eta$. On the other hand, Zohar & Ho (1996) obtained in a turbulent mixing layer $k_d/k_\eta = 0.1$. Champagne (1978) reported a similar ratio of 0.1 in a turbulent wake and a turbulent jet. Zohar & Ho (1996) found that the PVC scale is equal to the scale of maximum dissipation in a mixing layer. Hence, this relationship is tested in all three shear flows.

6.3. *The PVC length scale as a dissipation scale*

In order to check the relationship between the PVC length scale and the dissipation process, the dissipation spectra have to be calculated. The required spectra were estimated from the energy spectra as described above in a few locations across the three shear layers. The dissipation wavenumber, k_d, corresponding to the peak of the spectrum can be determined for each point in the flow. The wavenumber corresponding to the PVC scale, k_ζ, was also calculated at the same locations based on the PVC

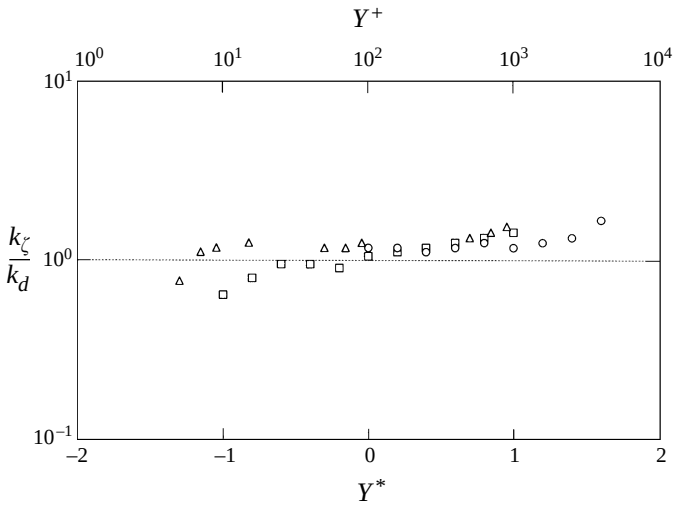

FIGURE 13. Cross-stream variations of the ratio between the PVC and the dissipation length scales for: △, boundary layer; ○, wake; □, mixing layer.

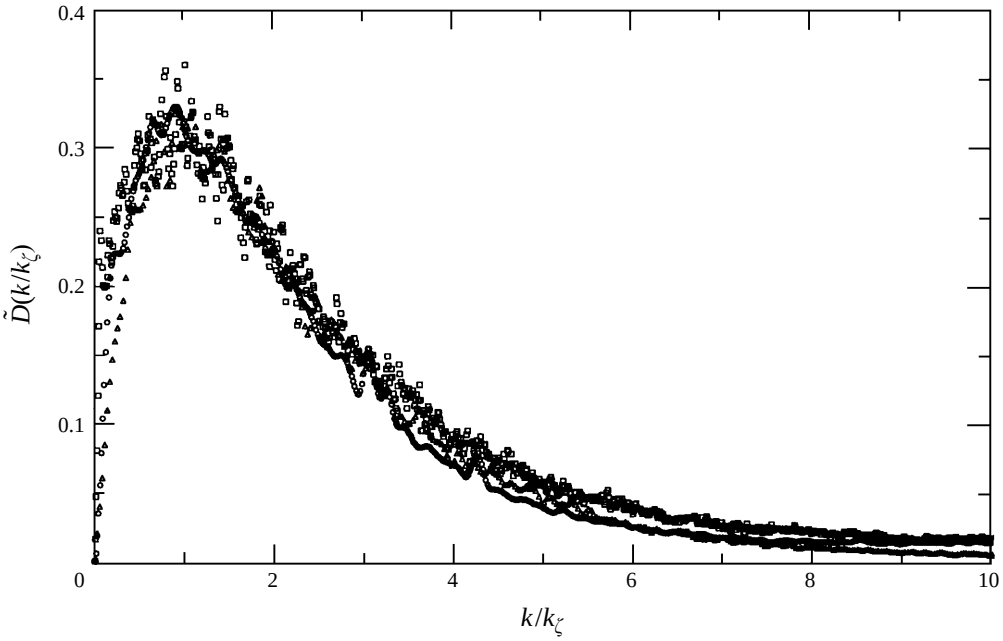

FIGURE 14. Normalized dissipation spectra for: △, boundary layer ($Y^+ = 70$); ○, wake ($Y^* = 1$); □, mixing layer ($Y^* = 0$).

histogram. The ratio k_ζ/k_d is plotted in figure 13 as a function of the cross-stream location, Y^+ for the boundary layer, Y^* for the wake and mixing layer. It is clear that inside the shear layers ζ is equal to the scale of maximum dissipation. Only at the edges, $|Y^*| > 1$ or $Y^+ > 10^3$, does the ratio k_ζ/k_d deviate somewhat from unity. This should be expected since at the edges of the shear layers the turbulent intermittency decreases. Now it is interesting to use k_ζ to normalize the dissipation spectrum. Figure 14 compares three spectra representing the three shear flows. The peak is indeed around

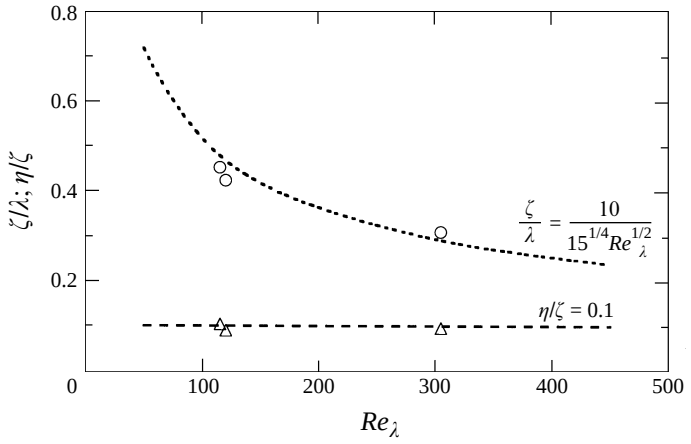

FIGURE 15. Re_λ dependence of the ratios between the microscales: $\triangle$, η/ζ; $\bigcirc$, ζ/λ.

$k/k_\zeta = 1$. Moreover, when the dissipation spectra are normalized by the total dissipation, $\int D(k)\,\mathrm{d}(k)$, such that the area enclosed by each spectrum is unity, all three dissipation spectra collapse together reasonably well. Thus it seems that the PVC technique yields the appropriate length scale for the dissipation process in turbulent shear layers.

6.4. *The relationship among turbulent microscales*

The relationship among the PVC scale ζ, the Kolmogorov microscale η, and the Taylor microscale λ is next examined. Figure 15 shows the ratio between the scales, ζ/λ and η/ζ, as a function of the turbulent Reynolds number, $Re_\lambda = \lambda u'/v$. Unfortunately, the range of Re_λ which can be investigated in this work is limited by the available facilities and is very small, 100–300, less than one order of magnitude. Nevertheless, the ratio between the Kolmogorov scale, η, and the PVC scale, ζ, does not seem to depend on Re_λ, at least within the limited range tested here. It is reasonable to expect that all the scales characterizing dissipative eddies would be proportional to each other. Therefore, the relationship between ζ and η can be written as

$$\zeta = a\eta, \tag{6.8}$$

where a should be a universal constant independent of Re_λ. Figure 15 shows that the best fit of (6.8) to the present data yields $a = 10$. In contrast, the relationship between the PVC scale and the Taylor scale λ should not be independent of Re_λ, because λ is not a scale characterizing fine eddies. The functional relationship between ζ/λ and Re_λ could be obtained as follows:

$$\frac{\zeta}{\lambda} = \frac{\zeta}{\eta}\frac{\eta}{\lambda} = \frac{10}{15^{1/4} Re_\lambda^{1/2}}. \tag{6.9}$$

This formulation, shown in figure 15, agrees well with the present data as ζ/λ decreases from about 0.45 for $Re_\lambda = 115$ and 120 in the wake and the boundary layer, respectively, to about 0.3 for $Re_\lambda = 305$ in the mixing layer.

7. Conclusions

The peak-valley-counting technique (PVC) has been developed to trace individual small-scale structures in turbulent flows. A detailed discussion of this technique is included in this paper. The main advantage in using the PVC technique is to alleviate

the noise contamination in the high-frequency range associated with high-order velocity derivatives. With this approach, it is possible to obtain a reliable most-probable length scale between zero-crossings of the first velocity derivative, ζ. This length scale is about equal to the wavelength at the peak of the dissipation spectrum. We have experimentally shown the generality of this property in three basic turbulent shear flows: a plane wake, a flat-plate boundary layer and a plane mixing layer. The ratio between ζ and the Taylor scale, λ, depends on the turbulent Reynolds number while the ratio between ζ and the Kolmogorov scale, η, is nearly constant. The proportionality constant between ζ and η was experimentally found to be about 10, different from the constant determined by analytical means.

We appreciate the many insightful comments made by the reviewers. Their comments have been incorporated in the present version. This work is supported by a contract from the Office of Naval Research.

REFERENCES

Acarlar, M. S. & Smith, C. R. 1987 A study of hairpin vortices in a laminar boundary layer. Part 2. Hairpin vortices generated by fluid injection. *J. Fluid Mech.* **175**, 43.

Batchelor, G. K. 1953 *The Theory of Homogeneous Turbulence*. Cambridge University Press.

Batchelor, G. K. & Townsend, A. A. 1947 Decay of vorticity in isotropic turbulence. *Proc. R. Soc. Lond.* A **190**, 534.

Batchelor, G. K. & Townsend, A. A. 1949 The nature of turbulent motion at large wave-numbers. *Proc. R. Soc. Lond.* A **199**, 238.

Blackwelder, R. F. & Haritonidis, J. H. 1983 Scaling of the bursting frequency in turbulent boundary layers. *J. Fluid Mech.* **132**, 87.

Brachet, M. E., Orszag, S. A., Nickel, B. G., Morf, R. H. & Frisch, U. 1983 Small-scale structure of the Taylor-Green vortex. *J. Fluid Mech.* **130**, 411.

Breidenthal, R. 1981 Structure in turbulent mixing layers and wakes using a chemical reaction. *J. Fluid Mech.* **109**, 1.

Browand, F. K. & Latigo, B. O. 1979 Growth of the two-dimensional mixing layer from a turbulent and a non-turbulent boundary layer. *Phys. Fluids* **22**, 1011.

Brown, G. L. & Roshko, A. 1974 On density effects and large structure in turbulent mixing layer. *J. Fluid Mech.* **64**, 775.

Brown, G. L. & Thomas, A. S. W. 1977 Large structure in a turbulent boundary layer. *Phys. Fluids Suppl.* **20**, S243.

Cantwell, B. J. 1981 Organized motion in turbulent flow. *Ann. Rev. Fluid Mech.* **13**, 457.

Champagne, F. H. 1978 The fine-scale structure of the turbulent velocity field. *J. Fluid Mech.* **86**, 67.

Crow, S. C. & Champagne, F. H. 1971 Orderly structure in jet turbulence. *J. Fluid Mech.* **48**, 547.

Favre, A., Gaviglio, J. & Dumas, R. 1967 Structure of velocity space-time correlations in a boundary layer. *Phys. Fluids Suppl.* **10**, S138.

Ferre, J. A., Mumford, J. C., Savill, A. M. & Giralt, F. 1990 Three-dimensional large-eddy motions and fine-scale activity in a plane turbulent wake. *J. Fluid Mech.* **210**, 371.

Foss, J. K. 1994 Small scale turbulence in a plane mixing layer. PhD thesis, University of Southern California, Los Angeles, CA.

Hinze, J. O. 1975 *Turbulence*. McGraw-Hill.

Ho, C. M. & Huang, L. S. 1982 Subharmonics and vortex merging in mixing layers. *J. Fluid Mech.* **119**, 443.

Ho, C. M. & Huerre, P. 1984 Perturbed free shear layers. *Ann. Rev. Fluid Mech.* **16**, 365.

Hsiao, F. B. 1985 Small scale transition and preferred mode in an initially laminar plane jet. PhD thesis, University of Southern California, Los Angeles, CA.

Huang, L. S. 1985 Small scale transition in a two-dimensional mixing layer. PhD thesis, University of Southern California, Los Angeles, CA.

Huang, L. S. & Ho, C. M. 1990 Small-scale transition in a plane mixing layer. *J. Fluid Mech.* **210**, 475.

Konrad, J. H. 1976 An experimental investigation of mixing in two-dimensional turbulent shear flows with applications to diffusion-limited chemical reactions. *Intern. Rep.* CIT-8-PU. Calif. Inst. Technol., Pasadena, CA.

Laufer, J. 1950 Some recent measurements in a two-dimensional turbulent channel. *J. Aero. Sci.* **17**, 277.

Lesieur, M. 1987 *Turbulence in Fluids*. Martinus Nijhoff.

Liepmann, H. W. 1949 Die anwendung eines satzes uber die nullstellen stochastischer funktionen auf turbulenzmessungen. *Helv. Phys. Acta* **22**, 119.

Liepmann, H. W., Laufer, J. C. & Liepmann, K. 1951 On the spectrum of isotropic turbulence. *NACA TN* 2473.

Liu, J. T. C. 1981 Interactions between large-scale coherent structures and fine-grained turbulence in free shear flows. In *Transition and Turbulence*, p. 167. Academic.

Longuet-Higgins, M. S. 1958 On the intervals between successive zeros of a random function. *Proc. R. Soc. Lond.* A **246**, 99.

Mattingly, G. E. & Criminale, W. O. 1972 The stability of an incompressible two-dimensional wake. *J. Fluid Mech.* **51**, 233.

Monin, A. S. & Yaglom, A. M. 1975 *Statistical Fluid Mechanics*, Vol. 2. MIT Press.

Monkewitz, P. A. & Huerre, P. 1982 The influence of the velocity ratio on the spatial instability of mixing layers. *Phys. Fluids* **25**, 1137.

Moser, R. D. & Rogers, M. M. 1993 The three-dimensional evolution of a plane mixing layer: pairing and transition to turbulence. *J. Fluid Mech.* **247**, 275.

Motohashi, T. & Blackwelder, R. F. 1983 Decreasing the side wall contamination in wind tunnels. *Trans. ASME: J. Fluids Engng.* **105**, 435.

Pao, Y. H. 1965 Structure of turbulent velocity and scalar fields at large wavenumbers. *Phys. Fluids* **8**, 1063.

Pierrehumbert, R. T. & Widnall, S. E. 1982 The two- and three-dimensional instabilities of a spatially periodic shear layer. *J. Fluid Mech.* **114**, 59.

Rice, S. O. 1945 Mathematical analysis of random noise. *Bell Syst. Tech. J.* **24**, 46.

Rogers, M. M. & Moser, R. D. 1992 The three-dimensional evolution of a plane mixing layer: the Kelvin–Helmholtz rollup. *J. Fluid Mech.* **243**, 183.

Roshko, A. 1981 The plane mixing layer flow visualization results and three dimensional effects. In *The Role of Coherent Structures in Modelling Turbulence and Mixing* (ed. J. Jīmenez). Springer.

Sreenivasan, K. R., Prabhu, A. & Narasimha, R. 1983 Zero-crossings in turbulent signals. *J. Fluid Mech.* **137**, 251.

Taylor, G. I. 1938 Production and dissipation of vorticity in a turbulent fluid. *Proc. R. Soc. Lond.* A **164**, 15.

Tennekes, H. & Lumley, J. L. 1972 *A First Course in Turbulence*. MIT Press.

Townsend, A. A. 1976 *The Structure of Turbulent Shear Flow*, 2nd Edn. Cambridge University Press.

Van Atta, C. 1991 Local isotropy of the smallest scales of turbulent scalar and velocity fields. *Proc. R. Soc. Lond.* A **434**, 139.

Winant, C. D. & Browand, F. K. 1974 Vortex pairing: The mechanism of turbulent mixing layer growth at moderate Reynolds number. *J. Fluid Mech.* **63**, 237.

Wygnanski, I., Champagne, F. & Marasli, B. 1986 On the large-scale structures in two-dimensional, small-deficit, turbulent wakes. *J. Fluid Mech.* **168**, 31.

Wygnanski, I. & Fiedler, H. E. 1970 The two-dimensional mixing region. *J. Fluid Mech.* **41**, 327.

Wyngaard, J. C. 1968 Measurement of small-scale turbulence structure with hot wires. *J. Sci. Instrum.* **1**, 1105.

Ylvisaker, N. D. 1965 The expected number of zeros of a stationary Gaussian process. *Ann. Math. Statist.* **36**, 1043.

ZOHAR, Y. 1990 Fine scale mixing in a plane mixing layer. PhD thesis, University of Southern California, Los Angeles, CA.

ZOHAR, Y. & HO, C. M. 1996 Dissipation scale and control of fine-scale turbulence in a plane mixing layer. *J. Fluid Mech.* **320**, 139.

ZOHAR, Y., MOSER, R. D., BUELL, J. C. & HO, C. M. 1990 Length scales and dissipation of fine eddies in a mixing layer. In *Studying Turbulence Using Numerical Simulation Databases-III. Proc. 1990 Summer Program of the Center for Turbulence Research*, p. 225. Stanford University.